Journal of Materials Science: Materials in Electronics (2019) 30:3530–3538
https://doi.org/10.1007/s10854-018-00630-0

Physical and optical properties of sprayed Cu_2ZnSnS_4 (CZTS) thin film: effect of Cu concentration

R. J. Deokate[1] · R. S. Kate[1] · S. C. Bulakhe[1]

Received: 20 October 2018 / Accepted: 21 December 2018 / Published online: 2 January 2019

Abstract
The crystallographic microstructural and optical properties of CZTS thin film have been investigated with influence of copper concentration in spray solution. The X-ray and Raman study carried out to the prepared CZTS thin films and attained pure kesterite phase. The results of microstructural properties such as crystallite size, *d*-spacing, microstrain, texture coefficient and standard deviation investigated. The prepared CZTS thin film shows very high optical absorption of the order of 10^5 cm^{-1} in the visible region and the optical band gap energy varied between 1.45 and 1.47 eV. This optical band gap tuning is most applicable for solar cells. By using the Wemple–DiDomenico (WDD) single oscillator model, the optical parameters were calculated such as single oscillator energy (E_0), dispersion energy (E_d), static refractive index (n_0), etc. Large values of optical conductivity (σ) give the promise to the solar cell application.

1 Introduction

The overpriced CIGS and CdTe solar cells are substituted that adopt rare earth elements such as In, Ga, Te and toxic Cd with the earth-abundant and non-toxic solar cell materials, the serious research is being worked out [1, 2]. Quaternary kesterite copper zinc tin chalcogenide Cu_2ZnSnS_4 (CZTS) thin film solar cells have been very fascinated material from last 10 years due to its optical direct band gap (~ 1.5 eV), which is closer to the required optical band gap for solar cell and large absorption coefficient ($> 10^4$ cm^{-1}) [3, 4]. The CZTS thin films have been prepared and studied physical properties with several deposition techniques such as sputtering [5, 6], chemical vapor deposition [7], sol–gel method [8], painting [9, 10], electrodeposition [11, 12], spray Pyrolysis [13–15]. Among all these techniques chemical spray pyrolysis technique is one of the most useful and simplest, reasonable, environmentally friendly, negligible waste of chemicals with utilization best efficiencies closer to 100% with large deposition area.

In CZTS thin film to achieve highly pure kesterite phase and high efficient photovoltaics with large crystallite size throughout the experiment, the elemental concentration variation is necessary. Numbers of articles are available on the structural properties of the CZTS thin films, also on the elemental composition variation. Via sequential electrodeposition method, CZTS based solar cells synthesized using different copper salt concentration in which sulfurization was carried out in elemental sulfur vapor atmosphere by Mkawi et al. and they found that there was increase in the grain size with the increase in copper concentration [16]. Bhosale et al. studied the variation of copper concentration on the structural and phase purity of the CZTS [17]. Kumar et al. [18] reported the increase in optical band gap with decrease in copper salt concentration in the solution at substrate temperature of 370 °C using the Spray pyrolysis technique (SPT). Camara et al. [19] synthesized copper rich CZTS nanoparticles by a simple hydrothermal method with different concentration ratios of sulfur and copper and investigated the better results. No any literature gives the detailed idea about the microstructural properties as well as optical properties with their dispersion parameters, dielectric constants, optical conductivity, etc. In this study, the effect of copper concentration on the crystallographic microstructural and optical properties of the Cu_2ZnSnS_4 (CZTS) thin film is reported. The optical properties of materials, such as dielectric functions $\varepsilon = \varepsilon_r + i\varepsilon_i$ and refractive indies $N = n + ik = [\varepsilon]^{1/2}$, dispersion parameters, optical conductivity (σ_{opt}), etc. are essential to improve and elevate PV device structure [19–21].

✉ R. J. Deokate
deokate2000@yahoo.co.in; rjdeokate@gamil.com

[1] Vidya Pratishthan's, Arts, Science and Commerce College, Baramati, MS 413 133, India

2 Experimental details

2.1 Film deposition and characterization

The Cu_2ZnSnS_4 thin films were deposited by chemical spray pyrolysis technique at optimized substrate temperature at 350 °C. The concentrations of zinc, Tin and sulfur are kept at optimized value of 0.25 M, 0.25 M and 0.40 M respectively and the concentration of copper is varied from 0.145 to 0.165 M by an interval of 0.05 [17]. To recompense the loss of sulfur during spray deposition, excess amount of sulfur is taken. The other experimental parameters such as nozzle to substrate distance, carrier gas, etc. and spray deposition set-up were steady [17]. X-ray diffractometer (XRD Bruker AXS D8 Advance Model) was used to study the structural and crystallographic properties of the films with the Cu-K_α ($\lambda = 1.5406$ Å) radiation source in 2θ range 20°–80°. At room temperature Raman scattering was performed using the micro-Raman spectrometer (Jobin–Yvon Lab RAM HR 800UV) with the excitation by 514.5 nm photons of 20 mW Argon ion laser. Uv–visible spectroscopy (UV-1800 Shimadzu Uv–Vis-NIR Spectrophotometer) in the wavelength range 200–1100 nm at room temperature was used to study the optical parameters.

3 Result and discussion

3.1 X-ray diffraction study

Figure 1 shows the X-ray diffraction patterns of CZTS thin film deposited for different Cu-concentrations. The major diffraction peaks corresponding to the Milar (h k l) planes (1 1 2), (2 2 0) and (3 1 2) are observed at 2θ° 28.47°, 47.42° and 56.24°, respectively. The observed results are matched with the standard results and confirmed the prepared thin films are polycrystalline CZTS with kesterite phase [22]. Absence of the impurity peaks and secondary phases gives the formation of the pure and good quality CZTS thin films and it is also confirmed by Raman analysis. Some authors have detected the other secondary phases (CdS, ZnS) in the CZTS thin film with variation of Cu concentration. The XRD patterns showed increase in peak intensity upto 0.155M cu-concentration as shown in the Fig. 2a. The maximum crystalline size value was observed for 0.155 M copper concentration and further decreased at higher copper concentration (0.165 M). Exactly opposite behaviour in full width at half maximum (FWHM) is observed due to the large grain formation at 0.155 M copper concentration. The calculated lattice parameters showed the values a = 5.42 Å and c = 10.84 Å and the value of c/2a is close to 1, indicates tetragonal unit cell [22].

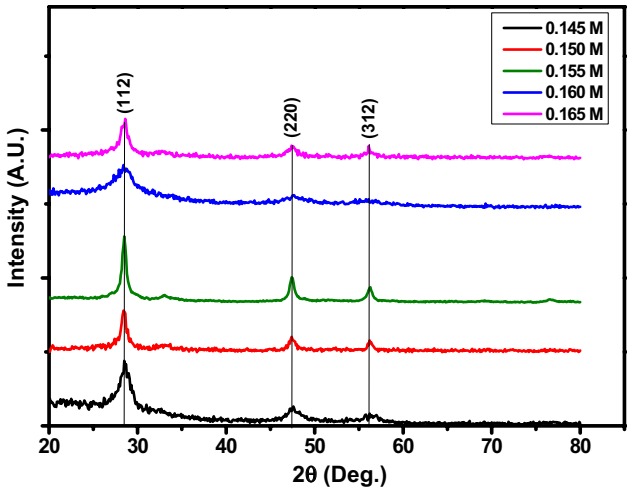

Fig. 1 X-ray diffraction analysis of CZTS thin films with different copper concentrations

The local distortion of the lattice planes due to the plastic deformation, interplaner spacing variation is calculated by microstrain (ε) using following formula [23]:

$$\varepsilon = \frac{\beta\cos\theta}{4} \tag{1}$$

where, β is the full width at half maximum (FWHM) of the prominent peak and θ is the half of the diffraction angle (2θ). The lattice (*d*-spacing) parameters were calculated by Bragg's diffraction equation. The microstrain indicated very smaller the variation in the lattice spacing and analogous results were observed for the prepared CZTS thin films. Figure 2b shows that, microstrain varied in the range 9.4×10^{-3} to 2×10^{-3}, change in the lattice spacing attributed to enhancement in crystal growth [24, 25]. The crystallite size (D) was calculated using Scherrer's formula and the dislocation density (δ) was obtained by calculating the reciprocal of the square of the crystallite size [26, 27]. Maximum crystallite size 16.67 nm was observed to the 0.155 M copper concentration representing least crystal defects and plastic deformations. As shown in Fig. 2c, dislocation density of the CZTS thin films with Cu-variation showed minimum value for 0.155 M copper precursor concentration.

The preferential orientation or the random growth of the polycrystals collected from the relative intensities of the XRD pattern calculated by the texture coefficient (TC_{hkl}) using the following [28]:

$$TC_{hkl} = \frac{\frac{I_{hkl}}{I_{0\,hkl}}}{\frac{1}{N}\sum_{N}\frac{I_{hkl}}{I_{0\,hkl}}} \tag{2}$$

where, I_{hkl} is the intensity count of the observed peak, I_{ohkl} is the corresponding standard relative intensity count from

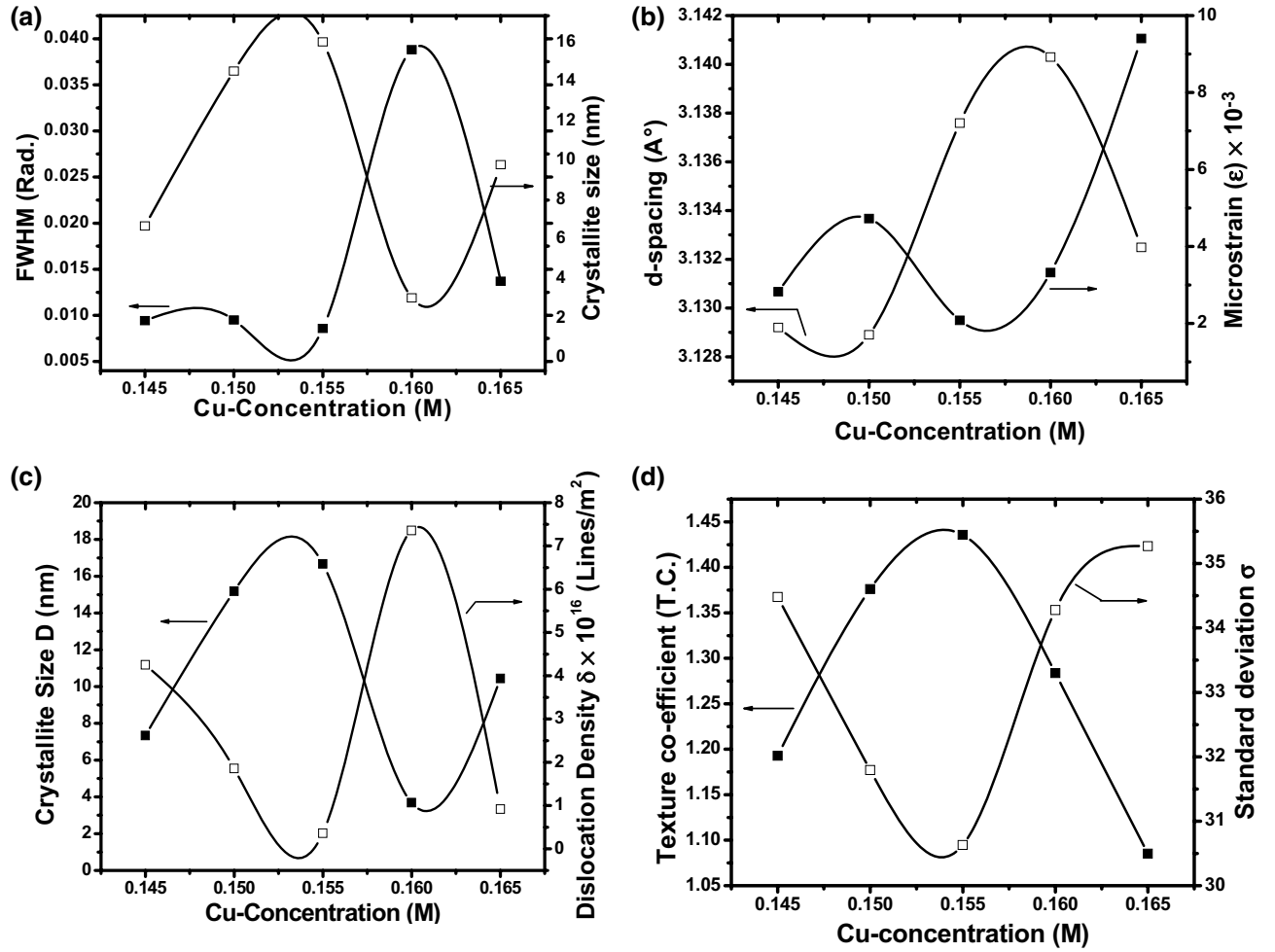

Fig. 2 **a** Variation of full width at half maximum and crystalline size of the CZTS thin films with different copper concentration, **b** interplaner spacing (d) and microstrain (ε) variation in the CZTS with the variation of copper concentration, **c** interrelation of crystallite size and dislocation density with various copper concentration, **d** effect of copper variation on the texture coefficient and standard deviation in the intensities of the peaks

the JCPDS data and *N* is the number of peaks of the planes observed in the pattern. The texture coefficient is greater than one when the *hkl*-planes are preferentially oriented. The lower values of the texture coefficient show poor crystallinity in the thin film and the CZTS thin film deposited with 0.155 M copper concentration gives maximum texture coefficient shown in Fig. 2d, which confirmed the maximum crystallite size for that particular copper concentration. The standard deviation (σ) in the intensities of various peaks was calculated to elucidate the growth mechanism of the CZTS films [29]:

$$\sigma = \sqrt{\frac{\sum_{N}(I)^2 - \frac{\left(\sum_{N} I\right)^2}{N}}{N}} \tag{3}$$

where, I is the relative intensity of the peak and N is the number of peaks observed. Figure 2d shows that standard deviation for various copper concentration which is found in the range between 34.48 and 30. The decrease in standard deviation was attributed to improved crystallinity and reorientational effects [30].

3.2 Raman spectroscopy study

Many secondary phases may appear in the quaternary kesterite compounds at the time of synthesis which may be affect on the grain growth, percentage phase purity, optical and electrical properties, solar cell property. Figure 3 gives the Raman spectroscopy analysis of CZTS thin films prepared for different copper concentrations. In Raman spectra peaks are observed, at 328 cm^{-1} with dominant peak and shoulder peak at 366 cm^{-1} which are basically of sulfur-kesterite

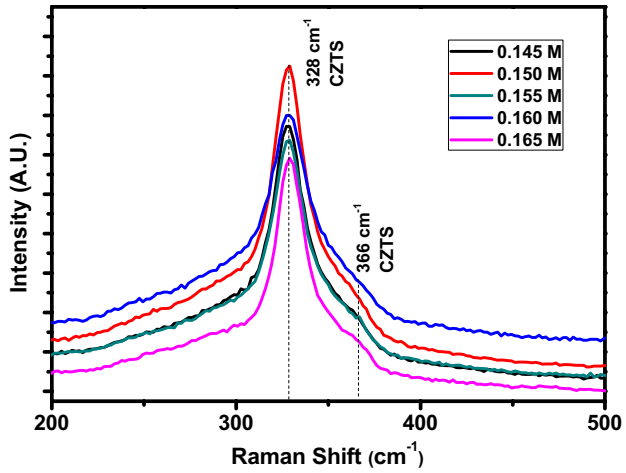

Fig. 3 Raman spectroscopy analysis of synthesized CZTS thin film with different copper concentrations

CZTS phase [31]. This observation is in agree with the XRD results The peak observed at 366 cm^{-1} is very week as compared to the strong Raman peak at 328 cm^{-1} corresponds to the preferential growth of the CZTS.

3.3 Optical spectroscopy study

The Fig. 4a shows the absorbance (A) spectra of the CZTS thin film which provides the relation between absorbance (A) and wavelength (λ). At shorter wavelength side (λ = 300–500 nm), maximum absorbance is observed and decreased continuously towards higher wavelength region (λ > 900 nm).

Figure 4b gives the transmittance (T) spectra of the CZTS thin films opposite to the absorbance, low transmittance at photons of shorter wavelength side and about 18% transmittance at longer wavelength side. The absorbance increased as

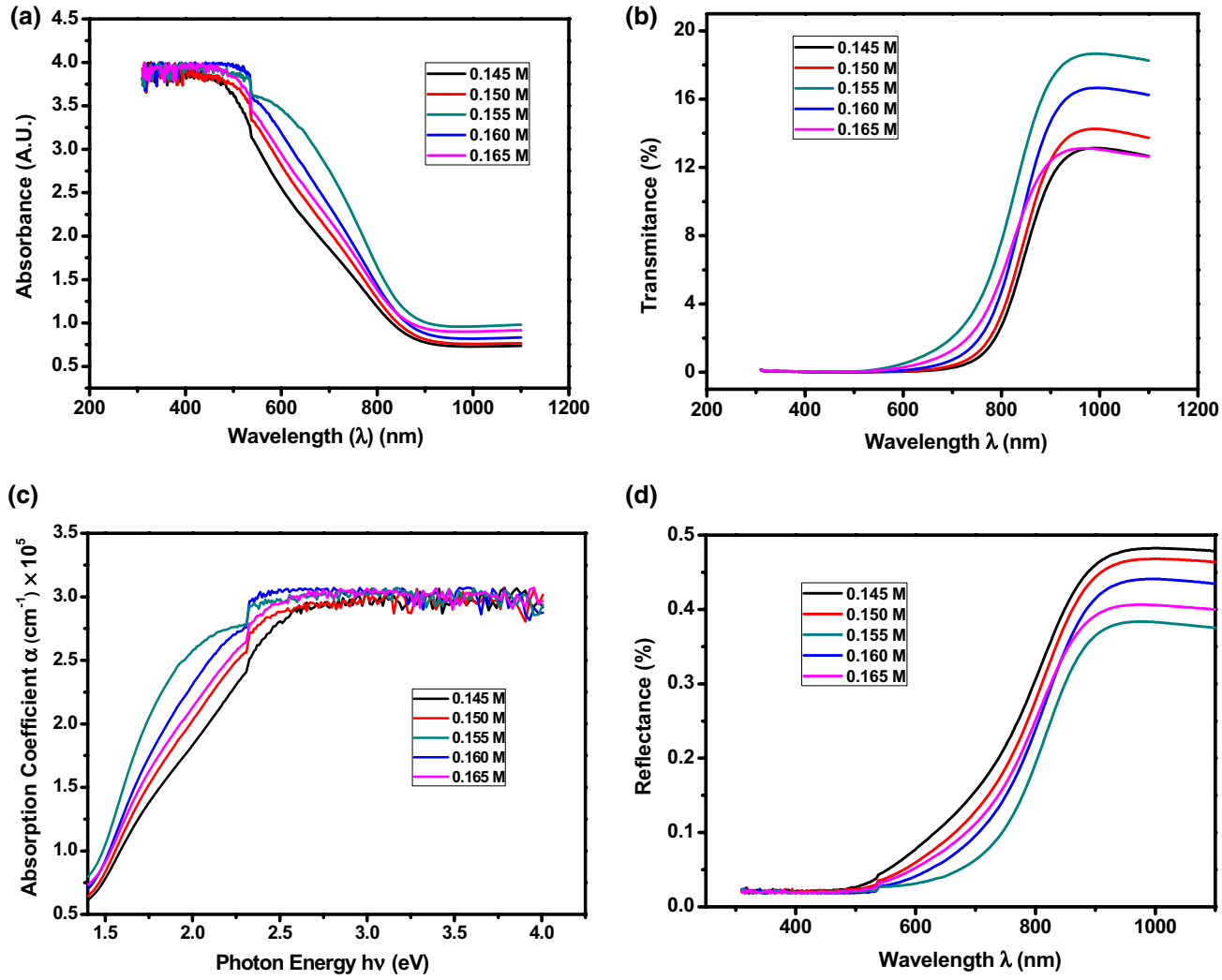

Fig. 4 **a** Absorbance (A) spectra of CZTS thin films, **b** transmittance (T) spectra of CZTS thin films, **c** the absorption coefficient (α) versus wavelength (λ) for the CZTS thin films, **d** reflectance (R) spectra of CZTS thin films

the concentration of the copper increased in the CZTS thin films and showed maximum for 0.155 M copper concentration further slightly decreased. From the transmittance and reflectance data, the absorption coefficient (α) was calculated by the relation [32, 33]:

$$\alpha = \frac{1}{d} \ln \left[\frac{(1-R)^2}{T} \right] \tag{4}$$

where, (R) is the reflectance, (T) is the transmittance and (d) is the thickness of the film. The change of absorption coefficient (α) with respect to the photon energy (hν) is shown in the Fig. 4c, which ascribes the synthesized CZTS thin films have very high absorption coefficient in the visible and near-IR region of the order of 10^5 cm^{-1}. This can be attributed to the increase in the probability of the occurrence of the direct transition [34].

Total reflectance of the CZTS thin film was calculated using the relation between absorbance (A), transmittance (T) and reflectance (R) as given bellow:

$$R = \left[1 - \left(\frac{T}{\exp(-A)} \right) \right]^{1/2} \tag{5}$$

The reflectance spectra for 0.145, 0.150, 0.155, 0.160 and 0.165 M copper concentration of CZTS thin films are shown in Fig. 4d and it reveals that the reflectance of all the thin films is < 0.5% in 300–1100 nm wavelength range. As the concentration of copper increases from 0.145 to 0.160 M in the CZTS thin films, the reflectance goes on decreased between 0.48–0.38% and again increased to 0.40% for higher copper concentration (0.165 M).

The plot of $(\alpha h\nu)^2$ versus (hν) shown in the Fig. 5a is the plot determining the optical band gap by the experimental values of absorption coefficient as a function of photon energy using Eq. (6) [35]:

$$(\alpha h\nu)^n = A(h\nu\text{-}E_g) \tag{6}$$

where, α is the absorption coefficient, hν is the photon energy, n is the exponent determines the type of electronic transitions causing the absorption and take the values 1/2 for indirect transitions and 2 for the direct transitions, A is the probabilistic parameter for the transition and E_g is the optical band gap energy. The optical band gap energy values observed between 1.45 and 1.47 eV and is in the range of required band gap value for the solar cell application [3, 4, 22, 36, 37]. For the lower copper concentration, band gap value has 1.45 eV and increases continuously with increase in copper concentration. Rendering to the equilibrium of the maximum of valence band and minimum of conduction band states, the band gap tunneling may be implicit [38]. With different compositions, the disorder between Cu and Zn cations is extremely likely in the CZTS semiconductors, and therefore its impact on the band gaps is also common [39].

The refractive index (n) of the CZTS thin films was calculated using the relation (7), where, R is the reflectance and (k_0) is the extinction coefficient which is measure of the fraction of light scattering loss and absorption per unit distance of the medium penetration of materials and calculated by using the relation (8) as given bellow [40]:

$$n = \frac{1+R}{1-R} + \left[\frac{4R}{(1-R)^2} - {k_0}^2 \right]^{1/2} \tag{7}$$

$$k_0 = \frac{\alpha \lambda}{4\pi} \tag{8}$$

Figure 5b gives the relation between extinction coefficient (k_0) and the wavelength (λ). Figure depicts the continuous variation in (k_0) over the wavelength range and shows maximum value at 500–650 nm and further decreased to higher wavelengths, resulting the direct relation is very easy to absorption of light. The lower values (0.004–0.013) indicated the strong absorbance of the CZTS thin films. Refractive index is an essential property of the material because it is related to the electronic polarizability of ion and local field inside the material in the design of heterostructure lasers in optoelectronic devices as well as in solar cell applications [41]. The plot of refractive index (n) versus photon energy (hν) is shown in Fig. 5c. Refractive index varies from 6 to 1.5 in the range of 1.1–2.5 eV photon energy (hν) and remains steady for higher photon energy. The higher values of refractive index attributed to the high crystallinity and densification of the thin films [42].

The single oscillator parameters as Wemple–DiDomenic dispersion parameter (E_0), dispersion energy (E_d), static refractive index (n_0), etc. can be calculated by the single oscillator model using the Wemple–DiDomenico (WDD) relation [43–46]:

$$n^2(h\nu) = 1 + \frac{E_0 E_d}{E_0^2 - (h\nu)^2} \tag{9}$$

where, (n) is the refractive index, (E_0) is the single oscillator energy, (E_d) is the dispersion energy which is the strength of inter band optical transition and (hν) is the photon energy. The values of E_0 and E_d can be found by plotting the graph of $(n^2-1)^{-1}$ versus $(h\nu)^2$ as shown in Fig. 5d, the intercept on Y-axis gives the value of E_0/E_d and the slope of the line gives the value of $1/(E_0E_d)$. The calculated values of E_0 and E_d are tabulated in the Table 1. Using these values (E_0 and E_d), the static refractive index (n_0) can be calculated by the formula:

$$n_0 = \sqrt{\left(1 + \frac{E_d}{E_0}\right)} \tag{10}$$

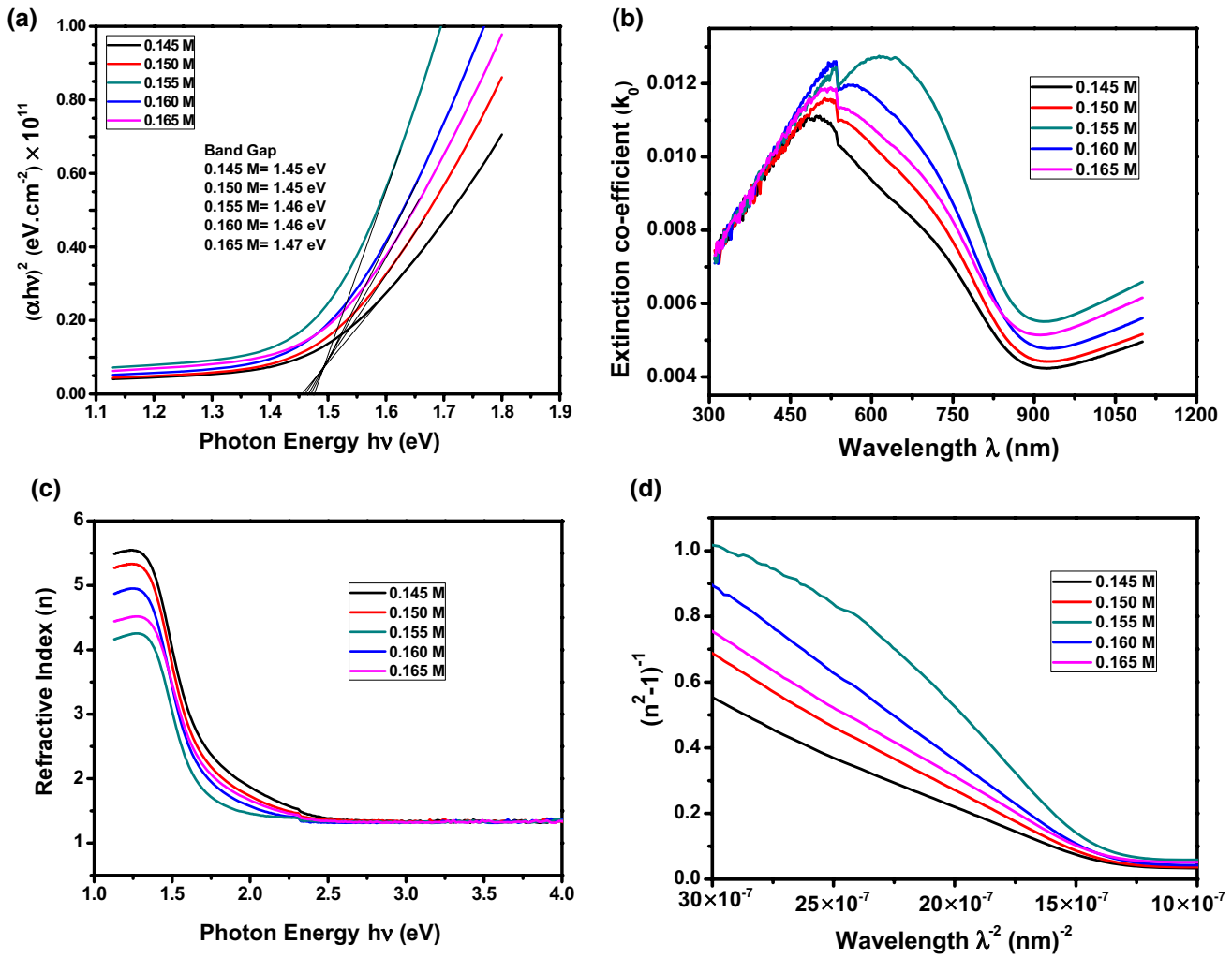

Fig. 5 **a** Plot of $(\alpha h\nu)^2$ versus photon energy ($h\nu$) of CZTS samples gives variation in optical band gap with different copper concentration, **b** the plot of extinction coefficient (k_0) versus wavelength (λ) for CZTS thin films, **c** refractive index (n) of CZTS thin films, **d** the plot of refractive index factor $(n^2 - 1)^{-1}$ versus reciprocal of square of wavelength

Table 1 The band gaps and the estimated values of the oscillator parameters E_0 and E_d as well as other related optical parameters extrapolated from WDD model

CZTS thin film	E_d (eV)	E_0 (eV)	n_0	E_g (eV)	E_0/E_g
0.145 M	2.41	1.34	1.67	1.45	0.92
0.150 M	1.94	1.33	1.56	1.45	0.91
0.155 M	1.45	1.30	1.45	1.46	0.89
0.160 M	1.38	1.40	1.40	1.46	0.95
0.165 M	1.75	1.32	1.52	1.47	0.89

The values of (n_0) can be calculated by extrapolating the Wemple–DiDomenico (WDD) equation (Eq. 9) to $h\nu \rightarrow 0$ and tabulated in Table 1.

The essential property of the optoelectronic semiconductor material is dielectric nature. There are two parts of dielectric constants; real part of dielectric constant (is to measure how much that material will slow down the speed of light) and imaginary part of dielectric constant (is to measure how a dielectric material absorbs energy from an electric field due to dipole motion). The real dielectric constant (ε_r) and imaginary dielectric constant (ε_i) can be calculated by using the values of refractive index (n) and extinction coefficient (k_0) by using the following relations [47–49]:

$$\varepsilon_r = (n^2 - {k_0}^2) \tag{11}$$

$$\varepsilon_i = 2nk_0 \tag{12}$$

Figure 6a and b gives the variation of (ε_r) and (ε_i) with respective of photon energy ($h\nu$), respectively. The values of the real dielectric constants are higher than the imaginary dielectric constants and both are decreases exponentially with increase in the photon energy. The optical

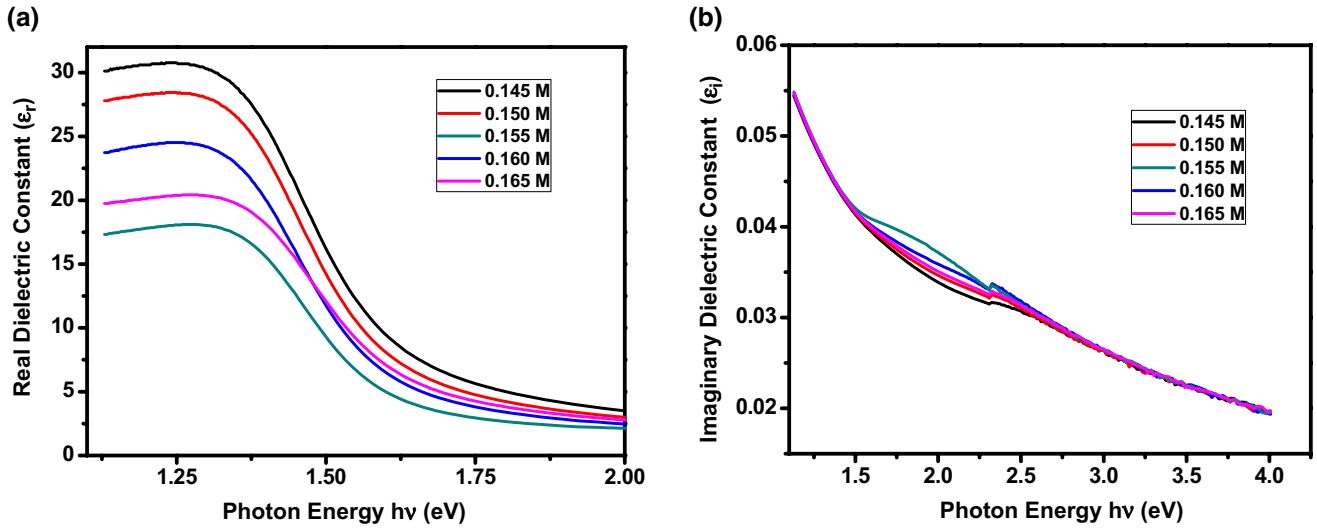

Fig. 6 **a** Variation of real dielectric constant (ε_r) with respect to photon energy ($h\nu$) of CZTS thin films, **b** variation of imaginary dielectric constant (ε_i) with respect to photon energy ($h\nu$) of CZTS thin films

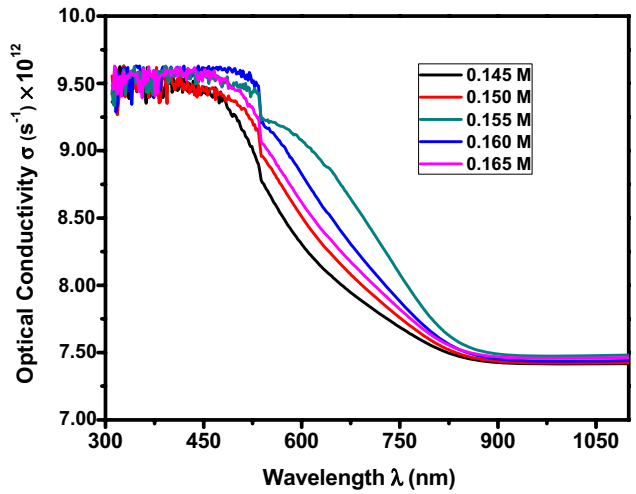

Fig. 7 Optical conductivity (σ) of CZTS thin films as a function of wavelength (λ)

response of a material is possibly deliberates in terms of optical conductivity. The optical conductivity of the material can be calculated by the relation, where c is the velocity of light [50]:

$$\sigma = \frac{\alpha n c}{4\pi} \tag{13}$$

Figure 7 gives the relation between optical conductivity (σ) and wavelength (λ). Figure showed the very large values (of the order of 10^{12} s^{-1}) of the optical conductivity in the lower wavelength (i.e. higher energy) range and slowly decreased from the absorption edge region to the longer wavelength. The large optical conductivity can be attributed to the excitation of the electrons due to high optical absorbance and low extinction coefficient [51].

4 Conclusions

In summary, the Cu_2ZnSnS_4 (CZTS) thin films were deposited by spray pyrolysis technique and reported the influence of copper concentration on the microstructural and optical properties. The X-ray diffraction and Raman spectroscopy analyses confirmed the pure kesterite CZTS phase with the expected results. The optical constants were confirmed by means of absorbance, transmittance and reflectance measurements at room temperature. The as synthesized CZTS thin films showed good optical absorption ($> 10^5$ cm^{-1}) in the visible region and the optical band gap energy in the range 1.45–1.47 eV. Fitting of the refractive indices rendering to the Wemple–DiDomenico (WDD) model, results in the dispersion of parameters that are directly related to the structural properties of the CZTS thin films.

Acknowledgements Authors are wishing thanks to the Science and Engineering Research Board, Department of Science and Technology (SERB/DST), New Delhi, India for their financial assistance through the fast track project (SB/FTP/PS-079/2014) titled "Fabrication of efficient Cu_2ZnSnS_4 (CZTS) thin film solar cells using economical Spray Pyrolysis".

References

1. C. Waida, A. Alivisatos, D. Kammen, Material availability expands the opportunity for large-scale photovoltaic development. Environ. Sci. Technol. **43**, 2072–2077 (2009)

2. M.A. Green, K. Emery, Y. Hishikawa, W. Warta, E.D. Dunlop, Solar cell efficiency tables (version 42). Prog. Photovolt. **21**, 827–837 (2013)
3. G. Larramona, S. Bourdais, A. Jacob, C. Chone, T. Muto, Y. Cuccaro, B. Delatouche, C. Moisan, D. Pere, G. Dennler, 8.6% Efficient CZTSSe solar cells sprayed from water–ethanol CZTS colloidal solutions. J. Phys. Chem. Lett. **5**, 3763–3767 (2014)
4. Q. Guo, S.J. Kim, M. Kar, W.N. Shafarman, R.W. Birkmire, E.A. Stach, R. Agrawal, H.W. Hillhouse, Development of $CuInSe_2$ nanocrystal and nanoring inks for low-cost solar cells. Nano Lett. **8**, 2982–2987 (2008)
5. H. Katagiri, K. Jimbo, W.S. Maw, K. Oishi, M. Yamazaki, H. Araki, A. Takeuchi, Development of CZTS-based thin film solar cells. Thin Solid Films **517**, 2455–2460 (2009)
6. J.J. Scragg, T. Ericson, T. Kubart, M. Edoff, C. Platzer-Björkman, Chemical insights into the instability of Cu_2ZnSnS_4 films during annealing. Chem. Mater. **23**, 4625–4633 (2011)
7. T. Washio, T. Shinji, S. Tajima, T. Fukano, T. Motohiro, K. Jimbo, H. Katagiri, 6% Efficiency Cu_2ZnSnS_4-based thin film solar cells using oxide precursors by open atmosphere type CVD. J. Mater. Chem. **22**, 4021–4024 (2012)
8. N. Kunihiko Tanaka, H. Moritake, Uchiki, Preparation of Cu_2ZnSnS_4 thin films by sulfurizing sol–gel deposited precursors. Sol. Energy Mater. Sol. Cells **91**, 1199–1201 (2007)
9. K. Woo, Y. Kim, J. Moon, A non-toxic, solution-processed, earth abundant absorbing layer for thin-film solar cells. Energy Environ. Sci. **5**, 5340–5345 (2012)
10. H. Zhou, H. Duan, W. Yang, Q. Chen, C. Hsu, W. Hsu, C. Chen, Y. Yang, Facile single-component precursor for Cu_2ZnSnS_4 with enhanced phase and composition controllability. Energy Environ. Sci. **7**, 998–1005 (2014)
11. S. Ahmed, K.B. Reuter, O. Gunawan, L. Guo, L.T. Romankiw, H. Deligianni, A high efficiency electrodeposited Cu_2ZnSnS_4 solar cell. Adv. Energy Mater. **2**, 253–259 (2012)
12. F. Jiang, S. Ikeda, T. Harada, M. Matsumura, Pure sulfide Cu_2ZnSnS_4 thin film solar cells fabricated by preheating an electrodeposited metallic stack. Adv. Energy Mater. **4**, 1301381 (2014)
13. S.A. Khalate, R.S. Kate, J.H. Kim, S.M. Pawar, R.J. Deokate, Effect of deposition temperature on the properties of Cu2ZnSnS4 (CZTS) thin films. Superlattices Microstruct. **103**, 335–342 (2017)
14. T.H. Nguyen, W. Septina, S. Fujikawa, F. Jiang, T. Harada, S. Ikeda, Cu_2ZnSnS_4 thin film solar cells with 5.8% of conversion efficiency obtained by a facile spray pyrolysis technique. RSC Adv. **5**, 77565–77571 (2015)
15. B. Dhruba, J.H. Khadka, Kim, Structural transition and band gap tuning of $Cu_2(Zn,Fe)SnS_4$ chalcogenide for photovoltaic application. J. Phys. Chem. C **118**, 14227–14237 (2014)
16. E.M. Mkawi, K. Ibrahim, M.K.M. Ali, A.S. Mohamed, Dependence of copper concentration on the properties of Cu_2ZnSnS_4 thin films prepared by electrochemical method. Int. J. Electrochem. Sci. **8**, 359–368 (2013)
17. S.M. Bhosale, M.P. Suryawanshi, J.H. Kim, A.V. Moholkar, Influence of copper concentration on sprayed CZTS thin films deposited at high temperature. Ceram. Int. **41**(7), 8299–8304 (2015)
18. Y.B.K. Kumar, G.S. Babu, P.U. Bhaskar, V.S. Raja, Preparation and characterization of spray-deposited Cu_2ZnSnS_4 thin films. Sol. Energy Mater. Sol. Cells **93**, 1230–1237 (2009)
19. S.M. Camara, L. Wang, X. Zhang, Easy hydrothermal preparation of Cu_2ZnSnS_4 (CZTS) nanoparticles for solar cell application. Nanotechnology **24**, 495401 (2013)
20. M. Law, M.C. Beard, S. Choi, J.M. Luther, M.C. Hanna, A.J. Nozik, Determining the internal quantum efficiency of PbSe nanocrystal solar cells with the aid of an optical model. Nano Lett. **8**, 3904–3910 (2008)
21. S.G. Choi, H.Y. Zhao, C. Persson, C.L. Perkins, A.L. Donohue, B. To, A.G. Norman, J. Li, I.L. Repins, Dielectric function spectra and critical-point energies of $Cu_2ZnSnSe_4$ from 0.5 to 9.0 eV. J. Appl. Phys. **111**, 033506 (2012)
22. JCPDS # 26-0575
23. E. G.Turgut, S. F.Keskenler.Aydin, S.Dogan, S.Duman, S.Özcelik, B. Gürbulakand, B. Esen, Fabrication and characterization of Al/Cu_2ZnSnS_4/n-Si/Al heterojunction photodiodes. Phys. Status Solidi A **211**, 580–586 (2014)
24. A. Moses Ezhil Raj, K.C. Lalithambika, V.S. Vidhya, G. Rajagopal, A. Thayumanavan, M. Jayachandran, C. Sanjeeviraja, Optical properties of Er^{3+}/Yb^{3+} codoped transparent PLZT ceramic. Phys. B: Condensed Matter **403**, 44–49 (2008)
25. J. He, L. Sun, K. Zhang, W. Wang, J. Jiang, Y. Chen, P. Yang, J. Chu, Effect of post-sulfurization on the composition, structure and optical properties of Cu2ZnSnS4 thin films deposited by sputtering from a single quaternary target. Appl. Surf. Sci. **264**, 133–138 (2013)
26. B.D. Cullity, *Elements of X-ray Diffraction* (Addison-Wesley, Palo Alto, 1956)
27. K.L. Chopra, T.F. Phenomena, *Thin Flim Phenomena* (McGraw-Hill, New York, 1969), p. 270
28. T.Massalski C.Bareet, *Structure of Metals* (Pergaron Press, Oxford, 1980), p. 1923
29. C. Agashe, M. Takwale, B. Marathe, V. Bhide, Structural properties of SnO_2: F films deposited by spray pyrolysis. Solar Energy Mater **17**, 99–117 (1988)
30. S.A. Khalate, R.S. Kate, H.M. Pathan, R.J. Deokate, Structural and electrochemical properties of spray deposited molybdenum trioxide (α-MoO3) thin films. J. Solid State Electrochem. **21**, 2737–2746 (2017)
31. R.M. Valls, T.S. Lyubenova, I.C. Roures, L. Oliveira, D.F. Chiva, J.B. Carda Castelló, Easy and low-cost aqueous precipitation method to obtain $Cu_2ZnSn(S, Se)_4$ thin layers. Solar Energy Mater. Solar Cells **161**, 432–438 (2017)
32. D.E. Milovzorov, A.M. Ali, T. Inokuma, Y. Kurata, T. Suzuki, S. Hasegawa, Optical properties of silicon nanocrystallites in polycrystalline silicon films prepared at low temperature by plasmaenhanced chemical vapor deposition. Thin Solid Films **382**, 47–55 (2001)
33. T.M. Wang, S.K. Zheng, W.C. Hao, C. Wang, Studies on photocatalytic activity and transmittance spectra of TiO_2 thin films prepared by r.f. Magnetron Sputtering Method. Surf. Coat. Technol. **155**, 141–145 (2002)
34. N.A. Bakr, Z.T. Khodair, S.A. Hassan, Effect of substrate temperature on structural and optical properties of Cu_2ZnSnS_4 (CZTS) films prepared by chemical spray pyrolysis method. Res. J. Chem. Sci. **5**(10), 51–61 (2015)
35. P. Kireev, *La Physique des semiconducteurs* (Mir, Moscou, 1975)
36. B.A. Schubert, B. Marsen, S. Cinque, T. Unold, R. Klenk, S. Schorr, H.W. Schock, Cu_2ZnSnS_4 thin film solar cells by fast coevaporation. Prog. Photovolt. Res. Appl. **19**, 93–96 (2011)
37. J.S. Seol, S.Y. Lee, J.C. Lee, H.D. Nam, K.H. Kim, Electrical and optical properties of Cu_2ZnSnS_4 thin films prepared by RF magnetron sputtering process. Sol. Energy Mater. Sol. Cells **75**, 155–162 (2003)
38. S.Y. Chen, A. Walsh, Y. Luo, J.H. Yang, X.G. Gong, S.H. Wei, Wurtzite-derived polytypes of kesterite and stannite quaternary chalcogenide semiconductors. Phys. Rev. B **82**, 195203 (2010)
39. F.J. Fan, L. Wu, M. Gong, G. Liu, Y.X. Wang, S.H. Yu, S. Chen, L.W. Wang, X.G. Gong, Composition- and band-gap-tunable synthesis of Wurtzite-derived $Cu_2ZnSn(S1–xSex)_4$ nanocrystals: theoretical and experimental insights. ACS Nano **7**, 1454–1463 (2013)

40. K.R. Nemade, S.A. Waghuley, Synthesis of MgO nanoparticles by solvent mixed spray pyrolysis technique for optical investigation. Int. J. Mater. (2014). https://doi.org/10.1155/2014/389416
41. R.R. Reddy, M. Ravi Kumar, T.V.R. Rao, Studies on the opto-electronic properties of alkali halides from optical electromagnetivities. Infrared Phys. **34**(1), 95–97 (1993)
42. N.A. Bakr, Characterization of a CdZnTe/CdTe heterostructure system prepared by Zn diffusion into a CdTe thin film. J. Cryst. Growth **235**(1), 217–223 (2002)
43. S.H. Wemple, M. DiDomenico, Behavior of the electronic dielectric constant in covalent and ionic materials. Phys. Rev. B **3**, 1338–1351 (1971)
44. N.A. Subrahamanyam, *A Textbook of Optics*, 9th edn. (Brj Laboratory, India, 1977)
45. K.S. Usha, R. Sivakumar, C. Sanjeeviraja, Optical constants and dispersion energy parameters of NiO thin films prepared by radio frequency magnetron sputtering technique. J. Appl. Phys. **114**, 123501 (2013)
46. A. Paliwal, A. Sharma, M. Tomar, V. Gupta, Optical properties of WO_3 thin films using surface plasmon resonance technique. J. Appl. Phys. **115**, 043104 (2014)
47. K. Punitha, R. Sivakumar, C. Sanjeeviraja, Pulsing frequency induced change in optical constants and dispersion energy parameters of WO_3 films grown by pulsed direct current magnetron sputtering. J. Appl. Phys. **115**, 2 (2014)
48. C. Kittel, *Introduction to Solid State Physics*, 7th edn. (John Wiley & Sons Inc., Singapore, 1996), pp. 307–308
49. A. Goswami, *Thin Film Fundamentals* (New Age International (P) Ltd., New Delhi, 2006), p. 376
50. I.C. Ndukwe, Solution growth, characterization and applications of zinc sulphide thin films. Solar Energy Mater. Solar Cells **40**, 123 (1996)
51. B. Ouni, A. Boukhachem, S. Dabbous, A. Amlouk, K. Boubaker, M. Amlouk, Some transparent semi-conductor metal oxides: comparative investigations in terms of Wemple–DiDomenico parameters, mechanical performance and Amlouk–Boubaker opto-thermal expansivity. Mater. Sci. Semicond. Process. **13**, 281–287 (2010)